Electric field strengths, ion energy distributions, and ion density decay for low-pressure, moderate-current nitrogen discharges

Jacek Borysow
Joint Institute for Laboratory Astrophysics, University of Colorado and National Institute of Standards and Technology, Boulder, Colorado 80309-0440
and Physics Department, Michigan Technological University, Houghton, Michigan 49931

A. V. Phelps
Joint Institute for Laboratory Astrophysics, University of Colorado and National Institute of Standards and Technology, Boulder, Colorado 80309-0440
(Received 4 January 1994)

Steady-state and time-dependent electric fields, ion densities, and ion velocity distributions are measured in the positive column of pulsed discharges in N_2 for conditions of moderate energy input per molecule, i.e., 0.1 eV/molecule. A nonintrusive laser absorption technique is used to determine axial velocity distributions of N_2^+ ions and the time dependence of the N_2^+ density from the shape and magnitude of absorption profiles of lines of the $A\,^2\Pi_u \leftarrow X\,^2\Sigma_g^+$ Meinel band of N_2^+. The discharges were operated at pressures from 0.3 to 1 Torr, electric field to gas density ratios E/n from 130 to 75 Td, pulse lengths of 10 to 20 μs, peak currents of about 1.5 A, and ion densities of 5×10^{17} ions/m^3. Here 1 Td $= 10^{-21}$ V m^2 and 1 Torr = 133 Pa. The line profiles were found to be consistent with the convolution of a theoretical, high field velocity distribution appropriate to charge transfer collisions and an above-thermal Maxwellian distribution. The electric field strength to gas density ratios E/n determined from the ion drift velocities are significantly lower than the predictions of the theory for a cold gas and suggest high ionization rates resulting from vibrationally excited N_2. The N_2^+ density decay following the pulsed discharge is consistent with ion loss by electron-ion recombination and ambipolar diffusion for electrons heated by the vibrationally excited N_2 at a calculated vibrational temperature of about 1900 K. The discharge conditions are briefly discussed so as to indicate the dominant processes and data needed for detailed models.

PACS number(s): 52.80.Hc, 52.25.Fi, 82.40.Ra

I. INTRODUCTION

Quantitative measurements of time-dependent electric fields, ion-velocity distributions, and ion densities provide the basis for developing and testing models of moderate-energy input, pulsed discharges in molecular gases. Such experiments and models provide improved understanding of a wide range of plasma phenomena, e.g., ambipolar diffusion, electron-ion collisions, energy transport, etc., and atomic and molecular collision processes, e.g., electron impact excitation, dissociative recombination, excited state quenching, etc. [1]. This paper is concerned with providing the data needed to test models of the axial electric field, the ion velocity distribution, and the decay of ion density in the early afterglow. The conditions in the discharge and afterglow are briefly modeled so as to provide an understanding of the dominant processes and guidance to future experiments and detailed theory.

A model of particular relevance to the present work is that of Dhali and Low [2] for pulsed discharges in N_2. Unfortunately, there were no experimental data for comparison with the model. Other recent models of pulsed discharges in nitrogen include that of Berdyshev *et al.* [3] for longer pulse lengths and higher pressures and that of Nagpal and Garscadden [4]. Recent models of dc discharges in N_2 include those of Loureiro *et al.* [5], Nagpal and Ghosh [6], and Alexandrov and Kochetov [7]. Recent models of the afterglow of pulsed discharges in N_2 include those of Colonna *et al.* [8] and Dyatko *et al.* [9]. Discharges of the type considered here occur in high power lasers [10], long-spark breakdown [11], the initial phases of lightning [12], and switching devices [13].

In the present experiments time-dependent electric fields and ion densities in low-pressure, positive-column electrical discharges and afterglows in N_2 and in N_2-He mixtures are determined using laser absorption measurements of the Doppler shifted line profiles for the $A\,^2\Pi_u \leftarrow X\,^2\Sigma_g^+$ Meinel transition of N_2^+ ions. In addition to the measurements of bulk discharge behavior, the measurements of the Doppler broadened absorption profiles make possible the first nonperturbative determinations of ion velocity distributions for ions moving in their parent gas. Previous measurements of the behavior of N_2^+ ions in discharges using laser techniques include measurements of ion drift velocities in the cathode fall region by Walkup, Dreyfus, and Avourios [14] and Gottscho *et al.* [15]. Ion-sampling measurements from N_2 discharges have also been reported [16] for the cathode region. The uniform-field drift tube in N_2 has been utilized by Duncan *et al.* [17] and Frost *et al.* [18] for measurements of rotational and vibrational excitation transfer in N_2^+ - He and N_2^+ - N_2 collisions.

Interest in electric field measurements stems from the

fact that one is now able to make rather sophisticated models of the motion of electrons and ions when the electric field to gas density ratio E/n is known. The electric field in a plasma is traditionally measured with a Langmuir probe, but this approach may perturb the plasma [19]. In recent years, there have been several nonintrusive measurements of the electric field in discharges using laser based techniques. Wieman and Hänsch [20] observed the Stark splitting in deuterium and hydrogen discharges. Doughty and Lawler [21] used the optogalvanic effect to measure Stark splitting for electric fields accurate to ± 10 V/cm at 400–1000 V/cm in helium discharges. Moore *et al.* [22] measured the electric field by observing the Stark mixing in an electronic transition of BCl. Ganguly *et al.* [23] applied the Stark splitting technique to very high levels of He excited by a laser from the metastable state. They used observation of resolved spectra for electric fields as low as 100 V/cm and observation of line merging for fields of ~ 5 V/cm. The Stark effect utilizing the NaK molecule was applied by Derouard and Sadeghi [24] to measurements of electric fields as low as 20 V/cm. Radunsky and Saykally [25] measured the time and spatially averaged electric fields in N_2-He discharges using a Doppler shift technique similar to that used in this work. Recently Booth *et al.* [26] used the Stark broadening of the H_δ line to determine the electric field in the sheath regions of low-frequency discharges. The present experiments were initially undertaken to determine the time dependence of the electric field strength during pulsed discharges and so test the proposal [27] that the change in electric field is responsible for the large variation in the apparent excited state production rate for pulsed N_2 discharges.

Previous experimental measurements of ion velocity distributions for ions moving in spatially uniform electric fields in the parent gas have utilized ion sampling at a negative electrode at high E/n with the resulting distortion of the ion energy distribution [28]. Infrared laser absorption measurements of the mean Doppler shift in the positive column of a dc discharge were used by Haese, Pan, and Oka [29] to obtain the mobility of ArH^+ ion in He. More recently, laser fluorescence measurements of ion velocity distributions have been used for studies of metallic ions in He [30,31] or molecular gas ions in He [18]. Bastien *et al.* [31] give a careful formulation of the relation between the observed fluorescence line profile and the ion velocity distribution that is applicable to absorption profiles.

The experimental arrangement for high spectral and time resolution measurements of the properties of the pulsed discharges is described in Sec. II. These techniques are an extension of those developed for the measurement of the collisional kinetics of H_2 ($c\,^3\Pi_u$) metastable states [32] and N_2 ($a''\ ^1\Sigma_g{}^+$) metastable states [27]. The techniques used to determine the electric field and velocity distribution of molecular ions in the positive column of a discharge are presented in Secs. III and IV. The measurement of ion density transients using the laser absorption technique is discussed in Sec. V. The present measurements have been summarized previously [33].

II. EXPERIMENTAL TECHNIQUE

The experimental technique used here is basically the same as that described earlier for the measurement of the kinetics of H_2 [32] and N_2 [27] molecular metastable states. A schematic of the discharge tube, the laser paths, and the detectors is shown in Fig. 1. The arrangement of the remainder of the optics and the electrical components is shown in Fig. 2 of Ref. [27]. A high density of $N_2{}^+$ ions, e.g., $\approx 5 \times 10^{17}$ m^{-3}, is produced in an axially uniform electric field in N_2 using a short-pulse positive column discharge. The discharge tube is in the form of a cross so as to remove the two cathode regions from the absorption path. The length of a single pass of the laser through the positive column is normally 200 ± 20 mm. Aluminum electrodes are used to reduce sputtering [34].

The discharge is operated at pressures of 0.3 to 1.5 Torr, pulse currents of 0.5 to 1.5 A, discharge pulse durations of 10 to 20 μs, and positive column electric fields of 10 to 30 V/cm. The voltage pulse was about 900 V and a series resistor of ~ 500 Ω was used to limit the current. Representative electric field, current, and 391.4 nm emission wave forms are shown in Fig. 2. Here the electric field is the measured difference between the voltage-probe wave forms discussed below divided by the electrode separation. A low repetition rate of 10 Hz–100 Hz ensures that the translational and rotational temperatures will return to close to the wall temperature between pulses. The wall temperature rise is calculated to be less than 15 °C [35]. As discussed in Sec. V and in the Appendix there may be a buildup of the vibrational temperature and the N atom density over a number of pulses.

The average electron-ion density is calculated from the

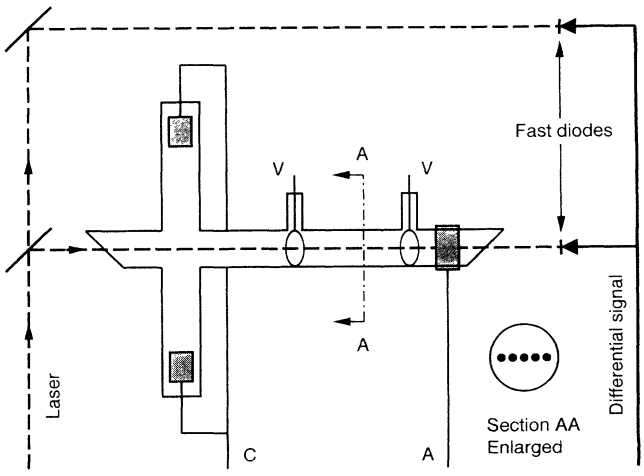

FIG. 1. Schematic of the experimental discharge tube used for Doppler shift and rotational population measurements in N_2. The solid circles in the section AA and the dashed line show the approximate location of the laser beams passing through the discharge. The arrows indicate the direction of the laser for the one-direction measurements. The voltage probes are labeled by V, the cathode connection by C, and the anode connection by A. The remainder of the circuitry and the optical system are described in Ref. [27].

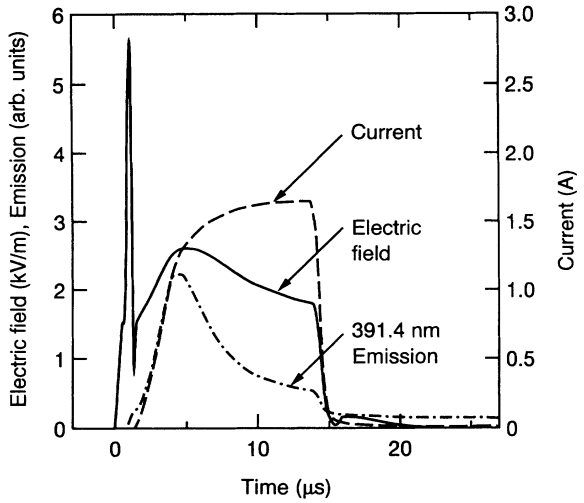

FIG. 2. Representative electric field, current, and 391.4 nm emission wave forms for $p = 0.75$ Torr and $I = 1.6$ A. Here time is measured from the beginning of the voltage pulse.

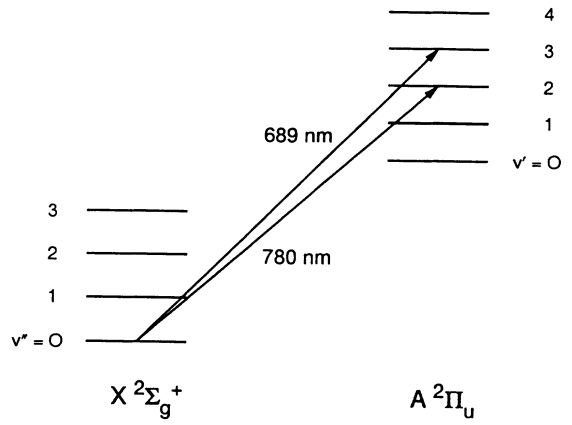

FIG. 3. Energy level diagram showing transitions of N_2^+ used in this paper. Lines of the Meinel band near 689 nm were used with the dye laser and lines of the Meinel band near 780 nm were used with the diode laser.

discharge current using the E/n values determined in Sec. III, published electron drift velocities [36], and assuming a Bessel function radial distribution of the electron and ion current density as expected for a diffusion dominated discharge. The estimated uncertainty in electron-ion density determinations is ±10% and arises from the uncertainty in measured current and radial current distribution. The duration of the discharge of 10–20 μs is chosen so that the ion density reached roughly its steady-state density at low currents [27]. Sometimes difficulty was encountered in operating the discharge in a reproducible fashion. The reproducibility improved when a small maintenance current was supplied using the circuit described earlier [37] for application of the dc and pulsed voltages. As shown in Fig. 2, the discharge current and light output do not show temporal oscillations during the pulse [38]. No spatial striation pattern [38] or evidence of a constricted discharge was observed. The reproducibility of the probe measurements was improved by placing a cylindrical (7 cm diam.) electrostatic shield around the discharge tube.

The N_2^+ energy levels and wavelengths [39,40] of interest in these experiments are shown in Fig. 3. The transition used depended on which of two laser systems was available.

(a) The original dye laser system [27,32] is based on an argon-ion-pumped cw dye (LDS 688) laser operating near 689 nm and with a bandwidth of about 1 MHz. This laser was used to measure absorption of lines of the $A\,^2\Pi_u \leftarrow X\,^2\Sigma_g^+$ ($v' = 3 \leftarrow v'' = 0$) band of N_2^+ [40].

(b) The newer tunable diode-laser system [41] with a linewidth < 1 MHz operated at wavelengths near 780 nm. The laser power incident on the sample was reduced to < 0.5 mW, compared to 10 mW available from the diode to avoid saturation effects and overloading the detector. The laser was tunable by variation in the effective length of the laser cavity over as much as 25 GHz at a fixed value of the electronically regulated [41] diode temperature (±0.001 K) and current ($\pm 10^{-5}$%).

We used this laser to measure absorption by lines of the $A\,^2\Pi_u \leftarrow X\,^2\Sigma_g^+$ ($v' = 2 \leftarrow v'' = 0$) band of N_2^+.

The laser beam is split so that one part is sent through the sample and one part is sent through the reference path. The beam passed through the sample cell from 3 to 7 times. In the "one-direction" experiments the beam path formed a loop so that the direction of propagation relative to the ion motion is fixed. In the "two-direction" experiments the beam is reflected nearly along the same path so that it alternated direction relative to the ion motion. The split beams are directed onto separate photodiodes connected in a differential bridge [27,32]. A variable attenuator in the reference path is adjusted such that the signals from the diodes were very nearly equal when the laser is tuned off resonance. Subtraction of the off-resonance signal from the on-resonance signal corrects for emission from the discharge. For line-profile measurements signals from the photodiodes are sent through a preamplifier and amplifier to a boxcar integrator operating in the active-base-line-subtraction mode. The bandpass of this signal processing electronics is normally from 0 to 160 MHz. For absorption transient measurements the signal is recorded with a 100 MHz transient digitizer. The total gain in the system amplifiers is usually 10^5.

The diode-laser system has a signal-to-noise ratio about 100 times that of the dye-laser system and allows measurement of absorption signals of less than 0.001% with a 0.5 μs time resolution or 0.005% with 50 ns time resolution. Using unpublished measurements of the absorption cross section [42], these limits correspond to N_2^+ densities of less than 2×10^{15} ions/m^3 and 10^{16} ion/m^3, respectively. For both lasers, the absolute frequency was measured using a moving-arm interferometer [43] that was accurate to 300 MHz with respect to a high quality, unstabilized He-Ne laser. A 7.5 GHz confocal étalon and diode served as a relative frequency marker.

The gas handling and vacuum system were unbaked, but could be pumped to $\sim 10^{-4}$ Pa ($\sim 10^{-6}$ Torr) between runs and when sealed off from the pumps had a rate of rise of $\sim 8 \times 10^{-5}$ Pa/s ($\sim 6 \times 10^{-7}$ Torr/s).

This rate of rise corresponds to $< 0.1\%$ impurities at the end of a 20 min run and is considered tolerable. The gas pressures were read with a diaphragm-type manometer rated accurate to $\pm$ 0.01 Torr. Currents and voltages are read from the digitized wave forms near the end of the current pulse and are expected to be accurate to $\pm 5\%$.

In addition to the electric field determinations using the Doppler shift methods discussed in Sec. III, the electric field strength in the pulsed N_2 discharges is determined using two Langmuir probes [19] operating at near their floating potentials and spaced 50 mm apart. In order to minimize the perturbation of the plasma, the probes are thin wire (0.2 mm) loops pressed against the glass wall of the discharge tube [27,32,44]. Our observation of no spatial dependence of the visual light emission in the vicinity of the probes is consistent with a small perturbation. The time-dependent voltages of the loops are measured using high impedance (100 MΩ) oscilloscope probes and the difference voltage determined by subtraction of the wave forms using a differential amplifier.

An important characteristic of the pulsed discharges used in these experiments is its uniformity in the axial direction. To test this uniformity, emission measurements were made from points at about 1 and 20 cm from the anode by observing the transient emission at 391.4 nm from the $B\,^2\Sigma_u^+ \rightarrow X\,^2\Sigma_g^+$ transition of N_2^+. Emission is measured with a photomultiplier using an interference filter centered at 391.4 nm with a 10 nm bandwidth. Care is taken to ensure that changes in the collection geometry are small. Emission transients taken at these positions are very similar. Since the excitation coefficient for the $B\,^2\Sigma$ state varies rapidly with E/n for these discharge conditions [45], this result is consistent with an electric field that is constant to $\pm 10\%$ along the discharge tube.

III. ELECTRIC FIELD IN THE POSITIVE COLUMN

The traces of Figs. 4 and 5 show representative absorption line profiles obtained with the diode laser and box-car integrator set for a few μs before the end of the current pulse when the electric field is $\approx$ 20 V/cm (solid curves) and set for a few μs after the end of the pulsed discharge when the electric field is small or zero (dashed curves). Both traces of Fig. 4 were obtained by passing the laser through the discharge cell 4 times in one direction. Such data will be referred to as one-direction data. The line is the $R_1(5)$ rovibrational line of the $A\,^2\Pi_u \leftarrow X\,^2\Sigma_g^+$ (v'=2, v''=0) transition [39,40] of the Meinel band of N_2^+. The center of the unshifted line is indicated by a vertical dashed line. Comparing the solid and dashed traces, one sees that in the presence of the pulsed electric field the ion line is shifted and asymmetric as a result of the drift of the ions towards the cathode. The details of the line profile will be discussed in this section and in Sec. IV A.

Figure 5 shows absorption wave forms obtained when the laser passed through the cell 5 times in both directions. Such data will be referred to as two-direction data. This arrangement results in a broadened line during the discharge, but produces no shift in the line center. The details of this line profile will be discussed in this section and in Sec. IV A. This technique was used in regions of the spectrum where the ion and neutral lines were badly overlapped and where it was desirable to sim-

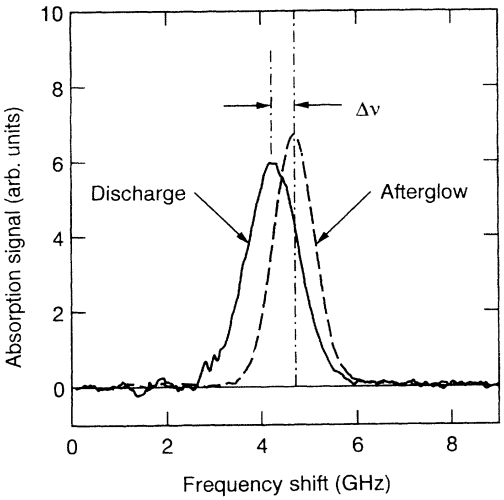

FIG. 4. Absorption signals for the $R_1(5)$ line of the $A\,^2\Pi_u \leftarrow X\,^2\Sigma_g^+$, $v' = 2 \leftarrow v'' = 0$ (Meinel) band at 381 465.0 GHz of N_2^+ using the one-direction laser path. The pulsed, positive column discharge is operated at a pressure of 0.3 Torr of N_2 and at a peak current of 1.5 A. The solid trace was taken near the end of the discharge, while the dashed trace was obtained early in the afterglow. The value of $\Delta\nu$ indicated is the mean frequency shift calculated using Eq. (1). The zero of frequency is arbitrary.

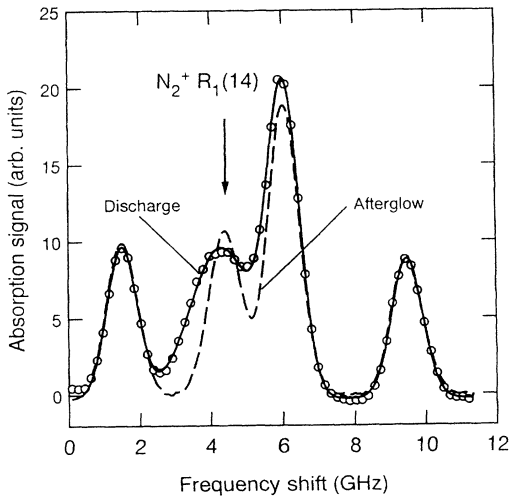

FIG. 5. Absorption signals for N_2^+ in pulsed discharge in N_2 obtained using the two-direction geometry. The arrow indicates the center of the $R_1(14)$ line of the $A\,^2\Pi_u \leftarrow X\,^2\Sigma_g^+$, $v' = 2 \leftarrow v''$=0 (Meinel) band of N_2^+ at 381 426.3 GHz. The other lines belong to the $B\,^3\Pi_u \leftarrow A\,^3\Sigma_u^+$, $v' = 7 \leftarrow v'' = 6$ (first positive) band of N_2. The left and center lines have been identified as $Q_{23}(9)$ and $R_{21}(3)$, respectively. The solid trace was taken near the end of the discharge, while the dashed trace was obtained early in the afterglow. The points show the fit of the set of theoretical Gaussian to the discharge data. p = 0.3 Torr and I = 1.5 A.

plify the fitting procedure. Absorption profiles for the $B\,^3\Pi_u \leftarrow A\,^3\Sigma_u$ transition, such as the three unchanged profiles shown in Fig. 5, yield a gas temperature of $\approx$ 370 K at the end of the discharge pulse. In the remainder of this section we discuss the determination of ion drift velocity and electric field from such data.

A. Data analysis methods

We have applied two methods of analyzing absorption profiles to obtain the frequency shift corresponding to the ion drift velocity.

1. Spectral moment method for one-direction data

This method is based on the calculation of mean frequency shift $\Delta\nu$ of the absorption line as the ratio of the first moment to the zeroth moment using the relation

$$\Delta\nu = \frac{\int d\nu(\nu-\nu_0)I(\nu-\nu_0)}{\int d\nu I(\nu-\nu_0)}\,, \qquad (1)$$

where ν_0 is the frequency of the line center as determined in the absence of an electric field and $I(\nu-\nu_0)$ is the measured absorption line profile. The frequency of the center of the unperturbed line ν_0 is assumed to be at the center of the absorption profile measured after the discharge voltage is reduced to zero, i.e., ν_0 is adjusted to make $\Delta\nu = 0$ in Eq. (1) for $I(\nu-\nu_0)$ taken after the end of the applied voltage pulse. An important advantage of this technique is that in the absence of overlapping lines no other measurements or fitting procedures are required to complete the analysis.

2. Convolution method

The convolution method assumes that the ion velocity distribution can be represented by the convolution of Gaussian profile corresponding approximately to the thermal motion of the ions and to a component of the velocity distribution applicable at high enough E/n so that the thermal motion of the gas can be neglected. See Sec. IV A for details of the model. This method can be applied to either one-direction or two-direction absorption data. The parameters of the velocity distribution plus those describing the background signal and absolute amplitude of the absorption signal are adjusted to give the best fit of the model to the measured line absorption profile.

The moment method has the major advantage that it does not require any assumptions as far as velocity distribution of ions is concerned and does not involve a complicated fitting procedure. It provides the mean Doppler frequency shift, which equals the drift velocity of the ions divided by the wavelength. On the other hand, the two-direction convolution method is a line fitting technique that can easily be applied for overlapping spectral lines. This feature is particularly useful for $N_2{}^+$ in N_2 where there are often large numbers of absorption lines in the spectral region of interest.

B. Results

The electric field to gas density values E/n for our pulsed positive column discharges are calculated from measured $N_2{}^+$ drift velocities W_+ using an empirical fit to published data [46] for $10 \le E/n \le 300$ given by

$$E/n = 9.6 \times (W_+/50)^{0.95}[1 + (W_+/1000)]^{0.9}\,, \qquad (2)$$

where n is the gas density, R is the radius of the discharge tube, E/n is in Td, and W_+ is in m/s. The resulting E/n values versus nR are shown by the solid circles in Fig. 6 for pressures from 0.25 Torr to 2.0 Torr and peak currents of 1.5 $\pm$ 0.1 A. The E/n results are plotted versus nR rather than pressure to allow scaling [38,44] of other measurements and with low-current positive column theory. The gas density in our experiments is calculated from the pressure assuming that the heated gas has not had time to expand significantly during our discharge pulse. This assumption is based on the transit time for sound across the tube and needs to be tested more thoroughly experimentally or estimated with a gas dynamic model. The decrease in longitudinal ion drift velocities with increasing radius caused by radial electric fields [47] is estimated to be less than about 3% in our measurements and is neglected.

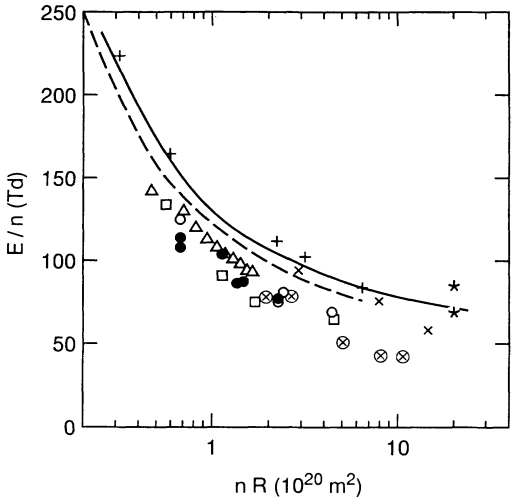

FIG. 6. Measured and calculated E/n versus nR for pure N_2 positive column discharges. The points are experimental results, while the smooth curves are calculated. Symbols and data sources include the following: •, Doppler shift from this paper; □, probe measurements from this paper; and △, probe measurements from Ref. [27] for $r = 7$ mm and a current pulse of 1.5 A. The points indicated by + are from Cernogora *et al.* [49] for $r = 7.5$ mm and a current of 1 mA. The points indicated by × and ⊗ are from Polak *et al.* [50] for $r = 8$ mm and dc currents of 5 and 75 mA, respectively. The points shown by * are from the model of Dhali and Low [2].

One source of error in pulsed discharge measurements is that there is sometimes a residual electric field after the applied voltage is turned off that is caused by circuit oscillations, etc. This field would result in a small Doppler shift in the dashed "reference" curve of Fig. 4 and a small excess width of the reference curve of Fig. 5. To test for such effects, we have measured absorption profiles at 1, 15, and 120 μs after the voltage pulse has been switched off. The frequency of the maximum of the $R(5)$ ion line in Fig. 4 decreases by about 35 MHz during the afterglow compared to the frequency shift of 480 MHz shown in Fig. 4 and compared to a full width at half maximum of about 1 GHz. From such data we estimate the uncertainty in the discharge E/n to be less than 10%.

C. Discussion of E/n results

The solid line of Fig. 6 shows the results of the steady-state electric field calculated theoretically using techniques previously applied to He-H_2 mixtures [44]. This model balances the loss of ions and electrons by ambipolar diffusion [48] against electron impact ionization [45] from ground state N_2. We have carried out the calculation for currents that are high enough (> 40 μA) so that charged particle loss is given by the limiting ambipolar diffusion model [48]. The calculation does not take into account the effects of excited states and so does not apply at the end of the discharge pulse at the high currents of the present experiments. The dashed curve of Fig. 6 shows the theoretical predictions of Cernogora *et al.* [49] using a similar model. The agreement with our solid curve is satisfactory given the differences in the assumed electron impact ionization coefficients.

The transient calculations of Dhali and Low [2] are more appropriate to our experiments. These authors find that for current densities a few times larger than our current densities the vibrational "temperature" T_v increases drastically at discharge times greater than about 100 μs. Because of the lack of experimental ionization coefficient data for $E/n < 85$ Td [36] and the difficulty of accurate calculations of ionization at low E/n [45], it is not surprising that their E/n value for a quasi-steady-state vibrationally cold N_2 discharge (the upper star in Fig. 6) is too high. The lower star in Fig. 6 is the Dhali and Low [2] result for a vibrationally hot, steady-state discharge in N_2 and is roughly 20% below their E/n for a quasi-steady-state vibrationally cold discharge. The time-dependent calculations of Nagpal and Garscadden [4] are for much lower current densities than those used in our experiments and are not easily compared with our results.

Figure 6 also shows electric field measurements obtained using the wire probes at times near the end of the pulsed discharges. Earlier results obtained with these probes [27] are shown as open triangles and the present results are shown by open squares. For the conditions of the present experiments, the voltage probe results are within $\pm 15\%$ of the laser absorption results and add to our overall confidence in the laser results.

The points shown by $\times$ and $\otimes$ in Fig. 6 are the E/n values on the discharge axis determined by Polak, Sergeev, and Slovetskii [50] for steady-state positive column discharges with nearly the same radius (8 mm) as for our pulsed discharge experiments. Note that these data are for much lower currents of from 5 to 75 mA and much longer times than our pulsed discharges. The times appropriate for comparison are some combination of the thermal diffusion time and the time for loss of vibrationally excitation, e.g., greater than about 200 μs from the Appendix. The pluses show the experimental steady-state results of Cernogora *et al.* [49] for currents of 1 mA. The results of these authors for high currents are not shown because of an unknown correction to the density for the gas temperature rise. Also, we have not shown the steady-state results of Güntherschulze [51] since we do not understand why his E/n values, especially at the lower nR and higher E/n, are so large compared to recent experimental results and to theory. Apparently the loss of charged particles is unusually fast in these experiments, possibly caused by electron-ion recombination or diffusion involving impurity ions.

Determinations of the electric field at different times during the pulsed discharge were made using the laser absorption method. Examples of such time-resolved E/n results are shown by the points with their uncertainty estimates in Fig. 7. These data were taken using the tunable, cw dye laser and have a considerably larger uncertainty than the data of Fig. 6. The time dependence of the electric field during the pulsed discharge determined from the probe measurements, such as shown by the solid curve in Fig. 7, is in qualitative agreement with the points of Fig. 7, but no probe data are available for a direct comparison with laser absorption data. If the

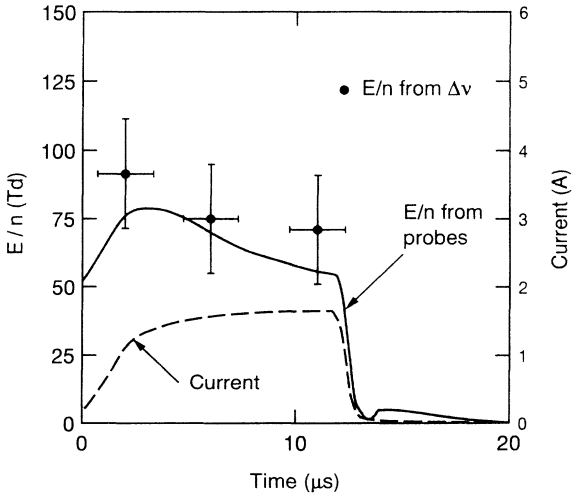

FIG. 7. Time dependence of E/n values obtained from mean Doppler shift during pulsed discharge for $p = 1$ Torr and $I = 1$ A. Here time is measured from the beginning of the current pulse. The solid curve shows E/n values calculated from probe measurements, while the dashed curve is the current wave form. These curves are for similar, but not identical, discharge conditions.

E/n determined from the laser absorption data are extrapolated to zero time, i.e., zero heating and excitation, we obtain significantly better agreement with the low-current theory shown by the solid line of Fig. 6. For example, the laser absorption data of Fig. 7 extrapolate to 100 ± 5 Td, while our low-current theory gives 105 Td.

For N_2^+ in He (not shown) the shifts in the frequencies of the ion lines are typically much larger than in the case of N_2^+ in N_2. For example, for $p = 1$ Torr, 5% N_2 in He, and $I = 1.55$ A, the frequency shift measured using the single-direction technique was 1.02 GHz corresponding to a drift velocity of 800 m/s. Using published drift velocity versus E/n data [46] for N_2^+ in He, we calculate a discharge E/n of 14 Td.

IV. VELOCITY DISTRIBUTION OF IONS

A. Velocity distributions at a fixed time

Little experimental or theoretical information is available regarding the velocity distribution of ions in their parent gas at moderate electric fields where the gain in ion velocity between collisions is comparable with the thermal velocity of the gas. Thus general solutions of the Boltzmann equation for ions in the presence of the charge transfer collisions and significant thermal motion do not appear to exist [52]. On the basis of our experimental results, we postulate that the velocity distribution of such ions is approximately given by the convolution of profiles appropriate to an "above-thermal" Maxwellian velocity distribution and a velocity distribution appropriate to high E/n or a "cold" gas. The full width at half maximum of the absorption line profile due to collision broadening is estimated to less than 5 MHz [53] and is neglected in this calculation of the line profiles.

The high-field or cold-gas approximation is obtained when thermal velocities can be neglected. We assume that the charge transfer cross section in N_2^+ collisions with N_2 is nearly independent of ion energy [54]. The solution [52,55] of the Boltzmann equation for the ion velocity distribution $h(\vec{v})$ then takes the form

$$h(\vec{v}) = C\delta(v_x)\delta(v_y)s(v_z)\exp\left[-\frac{n\sigma v_z^2}{2a}\right]$$

$$= F\delta(\Delta\nu_x)\delta(\Delta\nu_y)s(\Delta\nu_z)\exp\left[-\frac{n\sigma\lambda^2}{2a}\Delta v_z^2\right], \quad (3)$$

where v_x, v_y, and v_z are the x, y, and z components of the vector velocity; $\Delta\nu_x$, $\Delta\nu_y$, and $\Delta\nu_z$ are the corresponding frequency shifts, $s(v_z)$ and $s(\Delta\nu_z)$ are step functions; $\delta(v_m)$ is a delta function of the velocity component v_m; σ is the charge transfer cross section; $a \equiv eE/m$; e and m are the electronic charge and ion mass; and the electric field E is in the z direction. Here the v_m values have been converted into frequency shifts using the Doppler relation that

$$\nu - \nu_0 = v_z/\lambda_0 , \quad (4)$$

where ν_0 and λ_0 are the frequency and wavelength at the center of the unshifted molecular line. This distribution, shown by the dot-dashed curve in Fig. 8, reflects the assumption of the model that charge transfer collisions cause the N_2^+ ions to be left with zero velocity in the laboratory frame. This distribution is one-half of the Gaussian centered at zero velocity and having a half width at $1/e$ of the maximum equal to $v_z = (eE/mn\sigma)^{1/2} = (\pi/2)^{1/2}W_+$.

Theories of the motion of an atomic ion drifting through its parent gas and undergoing charge transfer collisions [52] show that the transport coefficients of He^+ in He are well represented by a "three-temperature" model, with effective temperatures describing a displaced Maxwellian velocity distribution in the field direction and a centered Maxwellian perpendicular to the field. Although such a model has not been applied to N_2^+ in N_2, we have tested the consistency of the displaced Maxwellian with experiment. The result of fitting a displaced Maxwellian or Gaussian representing the axial component of the velocity distribution to the experimental data (open points) is shown by the heavy dashed curve in the upper panel of Fig. 8. The smoothed differences between experiment and the theoretical profile are shown by the dashed curve in the lower panel of Fig. 8. Note that only every fourth experimental point is shown in Fig. 8. These plots show that while the bulk of the profile is consistent with the three-temperature model, there are significant discrepancies in the wings of the line that indicate the need for an asymmetrical line profile. All of our one-direction line profiles that have been fitted show this same asymmetry in the line wings. Similar discrep-

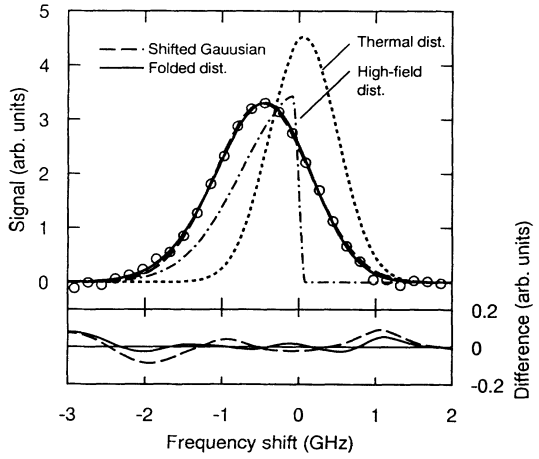

FIG. 8. The solid curve of the upper panel is the Doppler profile obtained by folding an above-thermal Maxwellian velocity distribution (not shown) and the theoretical high-field velocity distribution (dot-dashed curve). The dashed curve is the best fit of the Doppler profile predicted for a displaced Maxwellian velocity distribution. The points are experimental data obtained a few μs before the end of the discharge. The dotted curve is a fit of a Gaussian to experimental data for thermal ions obtained 120 μs after the discharge. The solid and dashed curves of the lower panel show smoothed differences between experiment and the corresponding best fit curves of the upper panel.

ancies with Monte Carlo calculations have been found for foreign gas ions drifting through a rare gas [56]. In this paper we neglect the possible dependence of the axial velocity distribution on the radial velocity, e.g., velocity component correlations such as found in Ref. [31]. The ion drift velocity obtained from this fit of a displaced Maxwellian is about 7% lower than the values obtained with the procedures of Sec. III or the fitting discussed in the following paragraph. This result is consistent with the missing high velocity ions in the shifted Maxwellian distribution.

The solid heavy curve of Fig. 8 shows that the discrepancies found with the three-temperature model can be significantly reduced by empirically calculating the line profile using an axial velocity distribution obtained by folding an unshifted, but above-thermal, Maxwellian component with an apparent ion temperature of 560 K into the high field distribution given by Eq. (3). The apparent temperature of this above-thermal axial component is comparable with the measured [57] effective temperature of the transverse component of $D/\mu = 0.047$ eV (corresponding to 540 K) at $E/n = 100$ Td, i.e., the above-thermal component of the velocity distribution is roughly isotropic. The above-thermal transverse component of the velocity distribution profile is expected to be enhanced by the large-angle ion-molecule scattering that occurs at low ion energies for which polarization scattering is important [58,59].

The lower panel of Fig. 8 compares the differences between the above-thermal high field line profile and experiment with the differences between the shifted Maxwellian profile and experiment. The ratio of standard deviations for the least-squares fits to the experimental profile of Fig. 8 for these two cases is 1.23:1. The difference data have been smoothed to clarify the regions of greatest difference. The region of frequency shift where the difference is largest corresponds to that of the fastest ions moving in the direction of acceleration by the electric field.

Since the relation between the apparent temperature of the above-thermal component of the axial velocity distribution and E/n is currently unknown, one can obtain the apparent temperature of the above-thermal component needed for analysis of two-directional measurements of Sec. III only by fitting one-directional experiments. For example, the use of the measured afterglow temperature in a folding type of analysis of two-directional data for a pressure of 0.3 Torr and a current of 1.5 A resulted in an E/n value that is 8% too high relative to the one-direction result. We have not investigated the variation of this error with pressure and E/n.

We have recorded line shapes and determined the drift velocity of N_2^+ in the positive column discharge for the rotational levels up to a quantum number 20 at pressures from 0.3 Torr to 1.5 Torr. We concluded that to within the experimental uncertainty of ±7%, the drift velocity of the N_2^+ in N_2 does not depend on the rotational quantum number of the molecular ion. The rotational temperature results derived from these measurements have been reported briefly elsewhere [60].

We also made measurements of Doppler profiles for N_2^+ in He. We find a good fit of a displaced Gaussian to the measured line profile. Although there appears to be no detailed theory for the velocity distribution of N_2^+ drifting in He, the displaced Gaussian found to fit the data is typical of experiment [30] for atomic ions in He. We find that the measured drift velocities are independent of the rotational quantum number up to 20. This result is to be compared with results for CO^+ ions in He [61,62], where the drift velocity increases with rotational level.

B. Transient behavior of the ion velocity distribution

Figure 9 shows transient absorption wave forms for various laser frequencies near the $R_{11}(11)A\,^2\Pi_u \leftarrow X\,^2\Sigma_g{}^+(v'=3 \leftarrow v''=0)$ transition of N_2^+ as obtained using the cw dye laser described in Sec. II. Here the detuning is measured from the frequency of peak absorption for the unperturbed line in the afterglow toward (and beyond) the frequency of peak absorption during the discharge. The bandwidth of the laser, the natural linewidth, and collision linewidth are significantly less than the Doppler width of the absorption line. Therefore measurements of absorption are sensitive to the small group of N_2^+ ions that have components of their velocity in the direction of propagation of the laser such as to match the Doppler-shifted laser frequency. At times near 17 μs in the upper traces of Fig. 9 one sees the cooling of the N_2^+ at the end of the discharge as a sharp change in absorption. From the observed lack of pressure dependence of such structure, we conclude that the velocity redistribution of N_2^+ ions in collisions with N_2 [63] is faster than the switching time of the discharge (≈ 1 μs). The lowest trace in Fig. 9 shows the transient absorption when the laser is tuned to observe absorption by fast ions. There is an appreciable number of ions in this velocity group when the electric field is on, but when

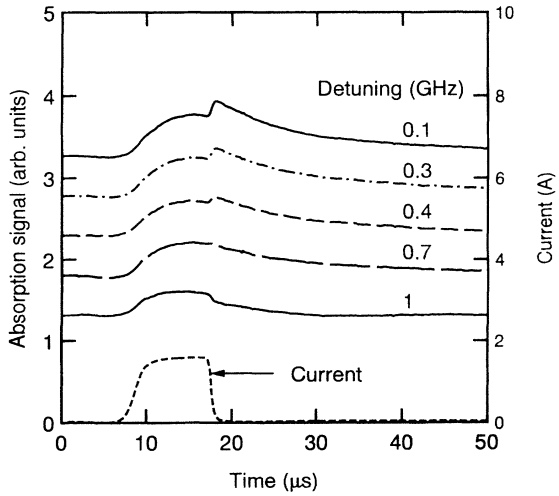

FIG. 9. Transient absorption by N_2^+ for various laser detunings. The upper trace is for the laser tuned near line center during the afterglow. The laser detuning toward the line wing increases for lower traces. The dashed curve shows the current transient. $p = 1$ Torr.

the discharge voltage and current are turned off, the ions suddenly slow down in collisions with cold N_2 and there is a decrease in the number of ions with the correct component of velocity.

V. TRANSIENT MEASUREMENTS OF ION DENSITY

In this section we compare the observed decay of N_2^+ ion density in the afterglow of the pulsed discharges considered in the preceding sections with a model including ion loss processes previously observed for discharges with lower energy input levels. These measurements utilized the absorption of the $R_1(4), A\,^2\Pi_u \leftarrow X\,^2\Sigma_g^+(v'=2 \leftarrow v''=0)$ transition with the diode laser operating near 780 nm. As discussed in Sec. III B, the absorption profile of the line changes little with time during the afterglow and the laser frequency can easily be set near the peak of the profile. We assume that the rotational and translational temperature is fixed during the afterglow, although the final time constant for the data of Fig. 10 is shorter than the thermal diffusion times given in Table I of the Appendix by only a factor of about 3. Thus we assume that the N_2^+ ion density is directly proportional to the measured absorption.

The representative absorption transient for N_2^+ shown in Fig. 10 is for a pressure of 0.3 Torr. The current wave form shown lasts for 12 μs and has a peak value of 1.55 A. The N_2^+ density wave form is an average [64] obtained with an effective time resolution of 0.8 μs. These data demonstrate the very high signal-to-noise ratio obtainable with the diode-laser absorption technique. The relative absorption measurements have been converted into absolute N_2^+ densities by assuming that the electron and ion densities do not change significantly as the electrons and ions cool after the discharge voltage is turned off, i.e.,

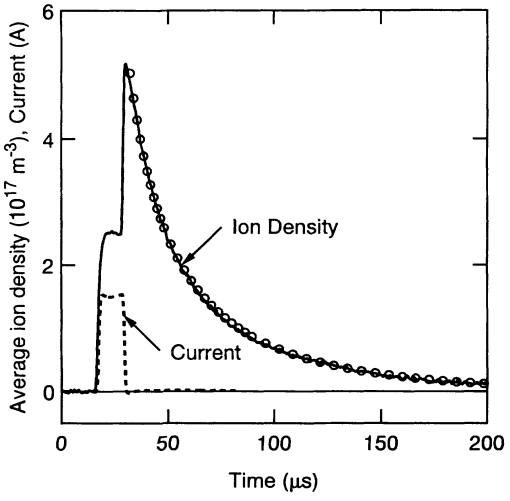

FIG. 10. Transient absorption by N_2^+ showing ion density decay during the afterglow of a pulsed discharge in N_2 for a pressure of 0.3 Torr. The solid curve is the normalized absorption data and the points are a fit of Eq. (6) to the experiment. The dashed curve shows the transient current.

that the electron density calculated from the measured discharge current and electron mobility vs E/n data [65] is equal to the ion density at the end of the discharge and at the beginning of the afterglow. This behavior follows from the slow change in ion density observed in Fig. 10 during the voltage-current decay shown in Fig. 2 and the small fractional difference in the electron and ion densities required to readjust the ambipolar electric field during the transition from discharge to afterglow [48].

The measured ion densities are such that losses due to dissociative recombination of electrons with N_2^+ [66,67], diffusion to the wall of the discharge tube [48], and N_2^+ to N_4^+ ion conversion [68] are expected to be of comparable importance. Electron–ion–neutral-particle recombination [69], radiative recombination [66,69], and collisional-radiative recombination [70] are expected to be negligible compared to dissociative recombination for our conditions. Our calculations show that the N_4^+ density has a negligible effect on the decay of the N_2^+ density [71], so that the error from assuming the N_2^+ density equals the electron density can be neglected.

Since an accurate model of spatially dependent decay of the N_2^+ density with all three loss processes active is difficult to solve [72], we consider an approximate solution in which the spatially dependent diffusion term is replaced by the fundamental mode spatial solution [48]. In this approximation, the N_2^+ density obeys the relation

$$\frac{dn_+}{dt} = -\alpha n_+^2 - \frac{(nD_a)}{n\Lambda^2} n_+ - k_c n^2 n_+ = -\alpha n_+^2 - \beta n_+ \,. \tag{5}$$

Here α is the dissociative recombination coefficient for N_2^+ and e, n_+ is the N_2^+ density, nD_a is the ambipolar diffusion coefficient at unit density, $\Lambda \equiv R/2.405$ is the fundamental-mode diffusion length, R is the tube radius, k_c is the three-body rate coefficient for conversion of N_2^+ to N_4^+, and $\beta \equiv (nD_a)/n\Lambda^2 + kn^2$. Ambipolar diffusion theory [48] shows that $nD_a = nD_+(1 + T_e/T_+) = n\mu_+(D_+/\mu_+)(1 + T_e/T_+)$, where nD_+ and $n\mu_+$ are the diffusion and mobility coefficients at unit gas density for N_2^+ in N_2 and kT_e/e and kT_+/e are the electron and ion temperatures, respectively. The errors resulting from the use of the simplified form of the diffusion term in Eq. (5) have been discussed by Frommhold and Biondi [72].

The solution to Eq. (5) for the N_2^+ ion density during the afterglow is

$$\frac{n_+(0)}{n_+(t)} = e^{\beta t} - \frac{\alpha n_+(0)}{\beta}\left[1 - e^{\beta t}\right] \,, \tag{6}$$

where $n_+(0)$ is the initial ion-electron density. The open points of Fig. 10 show the fit of Eq. (5) to the experimental data. In the fitting procedure the decay constant β, the product of the recombination coefficient α, and the initial ion density $n_+(0)$ were free parameters. The data of Fig. 10 yield $\alpha n_+(0) = 4 \times 10^4$ s^{-1} and $\beta = 1.17 \times 10^4$ s^{-1}. The average initial ion density $\langle n_+(0)\rangle$ calculated using the measured current and the electron drift velocity determined from the E/n value at the end of the discharge is 5.3×10^{17} m^{-3}, so that the "average" electron recombination coefficient is $\alpha = 9 \times 10^{-14}$ m^3/s. This re-

combination coefficient is significantly smaller than the value of 1.7×10^{-13} m^3/s measured [66,67] for 370 K electrons and N_2^+ ions.

The value of β for 370 K ions and electrons calculated from previous work is 4.9×10^3 s^{-1}. Here the ambipolar diffusion coefficient used is $nD_a = 3.2 \times 10^{20}$ m^{-1}s^{-1} based on ion drift velocity measurements [46] and thermal electron D/μ values [48]. The ion conversion coefficient used is $k_c = (4-8) \times 10^{-41}$ m^6/s from measurements in drift tubes [68]. Thus our experimental diffusion plus ion conversion loss is too large. A limited set of β determinations for various N_2 densities suggests that nD_a is $\geq 1.1 \times 10^{21}$ m^{-1}s^{-1} and that the ion conversion coefficient is $\leq 5 \times 10^{-42}$ m^6/s. Both a small recombination coefficient and a large diffusion coefficient are consistent with an electron temperature well above the gas temperature of 370 K. The $\approx$ 3:1 ratio of the apparent value of nD_a to the expected thermal value suggests that the electron temperature is $\approx$ 1800 K, i.e., comparable with the estimated vibrational temperature presented in Table I of the Appendix.

VI. DISCUSSION

The transient macroscopic electric fields determined for pulsed moderate current N_2 discharges using measurements of the N_2^+ absorption line profiles agree reasonably well with recent dc discharge experiments and roughly with the only available low-current model. Since the precision of the measurements of drift velocity is estimated to be better than a few percent and is comparable with the uncertainty of the published measurements of N_2^+ drift velocity versus E/n, we expect the uncertainty of the E/n determination to be better than $\pm 10\%$. This means that the observed scatter in the data of Fig. 6 is probably caused by changes in discharge operating conditions, e.g., current pulse initiation and wall reaction probabilities.

These experiments and analyses have shown that when the contribution to the velocity of the ions from the electric field is comparable with the thermal velocity, the convolution of the high field velocity distribution and a nonthermal Maxwellian distribution satisfactorily represents the velocity distribution and is much better than published three-temperature models at high ion energies. A proper representation of the ion energy distribution at high energies is of particular importance for the calculation of rates of ion-molecule reactions with a threshold energy significantly above the mean ion energy, e.g., vibrational excitation and N^+ and N_3^+ formation [54]. We have demonstrated that for N_2^+ in N_2 there is no dependence of the drift velocity on the rotational state of an ion. It remains to be seen whether the three temperatures of the model of Waldman, Vieland, and Mason [52] will agree with the results cited in Sec. IV when extended to describe the motion of N_2^+ in N_2.

The experiments and analyses presented in this paper show that in order to properly analyze high-current pulsed discharges in N_2 one needs to make simultaneous determinations of the N_2^+ and N_4^+ densities, the electric field, the N_2 translational temperature, N atom densities, and the vibrational temperature of the N_2. Other [3] studies have indicated the importance of measuring the various N_2 metastable densities in order to determine excitation and ionization processes and rates. Using the laser absorption technique we have measured the N_2^+ density, the electric field, and the N_2 translational temperature. Ershov and Borysow [73] have recently measured the vibrational temperature transient in such pulsed discharges. Since the N_4^+ ion absorbs and fluoresces in near ultraviolet [74] it may be possible to determine its density in a discharge by laser probe techniques.

Our original objective was to determine the source of the large decrease in N_2 $a''\,^1\Sigma_g^+$ metastable density during the later part of the pulsed discharge shown in Fig. 2 of Ref. [27] and the decrease in $N_2^+ B\,^2\Sigma_u^+$ emission shown in Fig. 2 of this paper. Calculated electron excitation coefficients for N_2 at 300 K [45] show that the reduction in E/n seen in Fig. 7 causes factors of 10 and 7 decreases the excitation rate coefficients for the $N_2^+ B\,^2\Sigma_u^+$ and $N_2 a''\,^1\Sigma_g^+$ states, respectively. These decreases during the discharge pulse are sufficient to cause the observed factor of 10 decrease in $N_2 a''\,^1\Sigma_g^+$ metastable density and the factor of 4 decrease in $N_2^+ B\,^2\Sigma_u^+$ emission. However, the analysis of the present experiment presented in the Appendix and other recent models [75,76] have shown that significant increases in the translational and vibrational temperatures of the N_2 are expected to occur during the discharge. The effect of the increase in the vibrational temperature on the relation between the N_2^+ drift velocity and E/n is small for our E/n [75], but the effect on these specific excitation coefficients of interest here has not been calculated. Judging from the calculated increase in the ionization rate coefficient for a vibrational temperature of 1900 K [76], the increase in excitation coefficients during the discharge pulse is less than a factor of 2. The effects of metastable states on the production of these excited states in our pulsed discharge has not been investigated, but probably is small because of the slow rise in metastable density during the discharge pulse.

ACKNOWLEDGMENTS

We would like to acknowledge the suggestion by R. A. Dressler that we use the Meinel band for our absorption measurements, the help and advice of K. Gibble in construction of the tunable-diode laser, and suggestions from A. Gallagher and J. Cooper in the course of the experiment. We would also like to thank S. J. Smith and J. Cooper for the loan of equipment and J. Fenney for help with the computer. The work was supported in part by the Air Force Wright Laboratories, the National Science Foundation, and by the National Institute of Standards and Technology.

APPENDIX: AFTERGLOW CONDITIONS

In this appendix we discuss the discharge conditions expected to prevail during the discharge and the after-

glow of the pulsed discharges used in the present experiments. Table I lists these discharge conditions for the three pressures and for the current and pulse duration at which most of the data were obtained. The determination of E/n values, electron densities, and translational-rotational temperatures from experimental data are discussed in Secs. III and IV.

The average energy input per molecule $\langle \Delta\epsilon \rangle$ at the end of the discharge is calculated from the relation

$$\langle \Delta\epsilon \rangle = \frac{(E/n) I \Delta\tau}{\pi R^2} \ . \tag{A1}$$

Here I is the discharge current, $\Delta\tau$ is the discharge pulse length, and R is the tube radius.

The energy stored as vibrational excitation $\langle \Delta\epsilon_v \rangle$ and the resultant vibrational temperature T_v are given by

$$\langle \Delta\epsilon_v \rangle = \frac{f_v \langle \Delta\epsilon \rangle}{[1 - \exp(-\tau_p/\tau_v)]} = \frac{\sum_m m\epsilon_v [\exp(-\epsilon_v/kT_v)]^m}{\sum_m [\exp(-\epsilon_v/kT_v)]^m} - \frac{\sum_m m\epsilon_v [\exp(-\epsilon_v/kT_g)]^m}{\sum_m [\exp(-\epsilon_v/kT_g)]^m} = \frac{\epsilon_v}{[\exp(\epsilon_v/kT_v) - 1]} - \frac{\epsilon_v}{[\exp(\epsilon_v/kT_g) - 1]} \ . \tag{A2}$$

Here ϵ_v is the excitation energy for the first vibrational level of N_2, f_v is the fractional power input to vibrational excitation from Refs. [45,65], T_g is the rotational-translational or "gas" temperature, k is the Boltzmann constant, Δt is the length of the discharge pulse, τ_v is the decay time for vibrationally excited N_2, and t_p is the time between pulses. In Eq. (A2) we make use of the harmonic oscillator approximation for the vibrational energy levels and assume that the discharge pulse length is short compared to τ_v.

The decay time for vibrationally excited N_2 in infinite cylindrical geometry is given by [77]

$$\tau_v = \frac{1}{D_v} \left[\Lambda^2 + \frac{R}{2\sqrt{3}} \frac{(2 - \gamma_v)}{\gamma_v} \frac{1}{nQ_v} \right] \ . \tag{A3}$$

The diffusion coefficient D_v and diffusion cross section Q_v for vibrationally excited N_2 are calculated from thermal

TABLE I. Discharge conditions for pulsed discharge and afterglow experiments.

Pressure (Torr)	0.3	0.5	1.0
Pulse current (A)	1.5	1.5	1.5
Pulse duration (μs)	15	15	15
At end of discharge			
E/n (Td)	110	103	77
Energy input/molecule $\langle \Delta\epsilon \rangle$ (eV)	0.10	0.09	0.07
Vibrational energy input (%)	60	68	85
Estimated average vibrational temperature (K)	1900	1900	1900
Translational-rotational T rise (K)	70[a]	70[b]	70[a]
Power input to translation and rotation (%)[c]	15	16	20
Increase in N during pulse (10^{17} m^{-3})[d]	2.5	7	0.9
Upper estimate of average N (10^{20} m^{-3})	1.6	1.3	0.3
Average electron-ion density (10^{17} m^{-3})	5.2	5.3	6.7
During afterglow			
Initial electron-ion density (10^{17} m^{-3})	5.2	5.3	6.7
Electron energy relaxation time (μs)[d]	8	5	2.5
Estimated τ_g relaxation time (μs)	140	220	430
Estimated τ_i relaxation time (μs)	0.9	0.6	0.3
Estimated τ_v relaxation time (s)	0.035	0.035	0.035
Estimated N atom density relaxation time (s) for $\gamma_v = 6 \times 10^{-6}$	1	1	1
Estimated N atom density relaxation time (s) for $\gamma_v = 1 \times 10^{-3}$	0.02	0.02	0.02
Apparent $\langle \alpha \rangle$ (10^{-13} m^3/s)	0.9	1.3	1.4

[a]Measured from neutral line profile.
[b]Interpolated between lower and higher pressure data.
[c]Calculated from measured neutral temperature rise.
[d]Calculated from excitation coefficients of Ref. [45].

conductivity data [78]. Because of the low probability γ_v usually found for vibrational deexcitation on striking the glass wall [79], i.e., $\gamma_v \approx 6\times10^{-4}$, the decay times for the vibrational temperature τ_v shown in Table I are long. As indicated in the first form of Eq. (A2) the energy stored in vibrationally excited N_2 is predicted to build up over a series of discharge pulses by an accumulation factor of $\{1 - \exp(-t_p/\tau_v)\}^{-1} \approx 1.1$ to 5 as the time between pulses t_p decreases from 0.1 to 0.01 s. Note that vibrational relaxation to translation in collisions with N_2 is slow [80]. Unfortunately, these present experiments yield only very indirect information regarding the vibrational temperature, i.e., the electron temperature discussed in Sec. V and below.

The thermal diffusion times given in Table I are calculated from Eq. (A3) by replacing γ_v and D_v with a $\gamma_T = 1$ as appropriate to a unit thermal accommodation probability at the wall and with a diffusion coefficient D_T calculated from the thermal conductivity [78]. Because of the large value of the accommodation coefficient, the calculated thermal decay times τ_g are much less than the time between discharge pulses t_p.

The fractional energy input that relaxes rapidly to the translational and rotational degrees of freedom of the N_2 at $E/n > 40$ Td has been discussed by several authors [45,75,76,81]. In particular, Gilmore [81] has reviewed the collisional kinetics of the electronically excited states. We note that the gas temperatures determined from the Doppler widths of the line of metastable N_2 shown in Table I correspond to the net fractional inputs of 20% and 15% at E/n of 77 and 110 Td. In order to obtain such low values from the rate coefficient calculations of Ref. [45] we need to assume that on our 15 μs time scale there is only a small quenching of the $A\,^3\Sigma$ metastables produced by electron excitation of the triplet system of N_2, that the radiating states of the singlet system of N_2 radiate rather than collisionally relax or predissociate, and that there is negligible vibrational relaxation.

The average electron density during the discharge is calculated from the discharge current I and the electron drift velocity W_e [45] using the relation

$$\langle n_e \rangle = \frac{I}{eW_e\pi R^2} \,. \tag{A4}$$

We assume that this electron density equals the ion density and is also the electron-ion density at the beginning of the afterglow.

The average density of nitrogen atoms $[N]$ is

$$[N] \approx \left(\frac{\alpha_d}{n}\right)\left(\frac{nI\Delta t}{e\pi R^2}\right)\left(\frac{\tau_N}{\tau_p}\right) \,. \tag{A5}$$

Here α_d/n is the rate coefficient for dissociation of N_2 by electrons normalized to the electron drift velocity and the gas density, τ_N is the decay time for the N atom density, and t_p is the time between discharge pulses. In Eq. (A5) we have assumed $\tau_N/\tau_p \gg 1$. The decay time τ_N for N atom density in N_2 is given by Eq. (A3) with the appropriate diffusion coefficient and cross section and a surface recombination probability for N atoms instead of the γ_v value for vibrationally excited N_2. We have used a normalized diffusion coefficient [82] of $nD = 7\times10^{20}$ m^{-1} s^{-1} for N and a corresponding cross section of $Q = 3\times10^{-19}$ m^2. If the probability of N atom recombination appropriate to the present experiments is as low as that generally obtained for a glass wall [83], i.e., $\gamma_N \approx 6\times10^{-6}$, the decay times of the atomic atom density are the long values given in Table I. In this case, the N atom density is predicted to build up over a series of discharge pulses by a factor up to 320. Because of the highly variable surface recombination probability [83], the N atom recombination at the aluminum anode could be negligible, as we have assumed in Table I, or it could be large and lead to a large reduction in the calculated N atom density from that shown in Table I. Kaufman [84] has suggested that the surface recombination probability for N atoms is 10^{-3} or larger for Pyrex glass exposed to an active discharge. In this case the values of τ_N would be much shorter than the values shown in Table I and the atom accumulation factor would be about 2.

[1] E. W. McDaniel, *Collision Phenomena in Ionized Gases* (Wiley, New York, 1964), Chaps. 5 and 12.

[2] S. K. Dhali and L. H. Low, J. Appl. Phys. **64**, 2917 (1988). Note that the electrode capacitance used by these authors ($\approx 6\times10^{-3}$ pF) is orders of magnitude smaller than the circuit capacitance in our experiment ($\approx$ 100 pF), so that our voltage rises relatively slowly and we do not see the initial plateau in the E/n and current wave forms given by their model.

[3] A. V. Berdyshev, I. V. Kochetov, and A. P. Napartovich, Fiz. Plazmy **14**, 741 (1988) [Sov. J. Plasma Phys. **14**, 438 (1988)].

[4] R. Nagpal and A. Garscadden (unpublished).

[5] J. Loureiro, C. M. Ferreira, M. Capitelli, C. Gorse, and M. Cacciatore, J. Phys. D **23**, 1371 (1990).

[6] R. Nagpal and P. K. Ghosh, Chem Phys. Lett. **183**, 129 (1991).

[7] N. L. Alexandrov and I. V. Kochetov, J. Phys. D **26**, 387 (1993).

[8] G. Colonna, C. Gorse, M. Capitelli, R. Winkler, and J. Wilhelm, Chem. Phys. Lett. **213**, 5 (1993).

[9] N. A. Dyatko, I. P. Kochetov, and A. P. Napartovich, J. Phys. D **26**, 418 (1993).

[10] B. E. Cherrington, *Gaseous Electronics and Gas Lasers* (Pergamon, Oxford, 1979), Chaps. 10–12.

[11] I. Gallimberti, J. Phys. (Paris) Colloq. **40**, C7-193 (1979); E. Marode, F. Bastien, and M. Bakker, J. Appl. Phys. **50**, 140 (1979); A. V. Eletskii and B. M. Smirnov, J. Phys. D **24**, 2175 (1991); J. J. Lowke, *ibid.* **25**, 202 (1992).

[12] M. A. Uman, *Lightning* (McGraw-Hill, New York, 1969), Chap. 5; M. N. Plooster, Phys. Fluids **14**, 2111 (1971); **14**, 2124 (1971).

[13] See, for example, J. Christiansen, in *Physics and Applications of Pseudosparks*, edited by M. A. Gundersen and G. Schaefer (Plenum, New York, 1990), p. 1, see also other papers in this conference proceedings.

[14] R. Walkup, R. W. Dreyfus, and Ph. Avouris, Phys. Rev. Lett. **50**, 1846 (1983).
[15] R. A. Gottscho, A. Mitchell, G. R. Scheller, Y.- Y. Chan, and D. B. Graves, Phys. Rev. A **40**, 6407 (1989).
[16] P. F. Knewstubb and A. W. Tickner, J. Chem. Phys. **37**, 2941 (1962); M. M. Shanin, *ibid.* **43**, 1798 (1965); A. V. Bonderenko, Zh. Tekh. Fiz. **45**, 308 (1975) [Sov. Phys. Tech. Phys. **20**, 195 (1975)].
[17] M. A. Duncan, V. M. Bierbaum, G. B. Ellison, and S. R. Leone, J. Chem. Phys. **79**, 5448 (1983); R. A. Dressler, H. Meyer, and S. R. Leone, *ibid.* **87**, 6029 (1987).
[18] M. J. Frost, S. Kato, V. M. Bierbaum, and S. R. Leone, J. Chem. Phys. **100**, 6359 (1994).
[19] J. F. Waymouth, J. Appl. Phys. **37**, 4492 (1966).
[20] C. Wieman and T. W. Hänsch, Phys. Rev. Lett. **36**, 1170 (1976).
[21] D. K. Doughty and J. E. Lawler, Appl. Phys. Lett. **45**, 611 (1984); D. K. Doughty, S. Salih, and J. E. Lawler, Phys. Lett. **103A**, 41 (1984).
[22] C. A. Moore, G. P. Davis, and R. A. Gottscho, Phys. Rev. Lett. **52**, 538 (1984); R. A. Gottscho, Phys. Rev. A **36**, 2233 (1987).
[23] B. N. Ganguly and A. Garscadden, Phys. Rev. A **32**, 2544 (1985); B. N. Ganguly, J. Appl. Phys. **60**, 571 (1986); B. N. Ganguly, J. R. Schoemaker, B. L. Preppernau, and A. Garscadden, *ibid.* **61**, 2778 (1987); J. R. Shoemaker, B. N. Ganguly, and A. Garscadden, Appl. Phys. Lett. **52**, 2019 (1988).
[24] J. Derouard and N. Sadeghi, IEEE Trans. Plasma Sci. **PS-14**, 515 (1986); H. Debontride, J. Derouard, P. Edel, R. Romestain, N. Sadeghi, and J. P. Boeuf, Phys. Rev. A **40**, 5208 (1989); M.-P. Alberta and J. Derouard, J. Phys. D **24**, 904 (1991).
[25] M. B. Radunsky and R. J. Saykally, Chem. Phys. Lett. **152**, 419 (1988). We are unable to make a quantitative comparison with these N_2-He results with ours because the radius of the discharge tube is not given.
[26] J.-P. Booth, J. Derouard, M. Fadlallah, and N. Sadeghi, J. Appl. Phys. **74**, 663 (1993).
[27] A. B. Wedding, J. Borysow, and A. V. Phelps, J. Chem. Phys. **98**, 6227 (1992).
[28] See, for example, T. Makabe and H. Shinada, J. Phys. D **18**, 2385 (1985); H. R. Skullerud and S. Holmstrøm, J. Phys. D **18**, 2375 (1985); M. J. Hogan and P. P. Ong, *ibid.* **19**, 2123 (1986).
[29] N. N. Haese, F.-S. Pan, and T. Oka, Phys. Rev. Lett. **50**, 1575 (1983)
[30] R. A. Dressler, J. P. M. Beijers, H. Meyer, S. M. Penn, V. M. Bierbaum, and S. R. Leone, J. Chem. Phys. **89**, 4707 (1988).
[31] M. J. Bastien, C. P. Lauenstein, V. M. Bierbaum, and S. R. Leone, J. Chem. Phys. **98**, 9496 (1993).
[32] H. Tischer and A. V. Phelps, Chem. Phys. Lett. **117**, 550 (1985); A. B. Wedding and A. V. Phelps, J. Chem. Phys. **89**, 2965 (1988).
[33] J. Borysow and A. V. Phelps, Bull. Am. Phys. Soc. **34**, 293 (1989).
[34] N. Laegreid and G. K. Wehner, J. Appl. Phys. **32**, 365 (1961).
[35] F. W. Sears and M. W. Zemansky, *University Physics* (Addison-Wesley, Reading, MA, 1970), p. 241.
[36] J. Dutton, J. Phys. Chem. Ref. Data **4**, 577 (1975).
[37] B. M. Jelenković and A. V. Phelps, Phys. Rev. A **36**, 5310 (1987).
[38] M. J. Druyvesteyn and F. M. Penning, Rev. Mod. Phys. **12**, 87 (1940).
[39] A. Lofthus and P. H. Krupenie, J. Phys. Chem. Ref. Data **6**, 113 (1977); T. A. Miller, T. Suzuki, and E. Hirota, J. Chem. Phys. **80**, 4671 (1984).
[40] G. H. Dieke and D. F. Heath, Johns Hopkins Spectroscopic Report No. 17, 1959 (unpublished). We thank W. Benesch for a copy of relevant portions of this report.
[41] K. Gibble and A. Gallagher, Phys. Rev. A **43**, 1366 (1991). We thank J. Hall for the circuit diagram and advice in the use of these devices. For one version see C. E. Wieman and L. Hollberg, Rev. Sci. Instrum. **62**, 1 (1991).
[42] Z. Lj. Petrović and A. V. Phelps (unpublished).
[43] J. L. Hall and S. A. Lee, Appl. Phys. Lett. **29**, 367 (1976).
[44] C. H. Muller, Jr. and A. V. Phelps, J. Appl. Phys. **51**, 6141 (1980).
[45] A. V. Phelps and L. C. Pitchford, Phys. Rev. **31**, 2932 (1985); A.V. Phelps and L.C. Pitchford, JILA Data Center Report No. 26, 1985 (unpublished).
[46] H. W. Ellis, R. Y. Pai, E. W. McDaniel, E. A. Mason, and L. A. Viehland, At. Data Nucl. Data Tables **17**, 177 (1976).
[47] C. C. Davis, Phys. Rev. A **32**, 3566 (1985). The radial electric fields present in our discharges for $p = 0.3$ Torr produce radial E/n of about 50 Td at $r/R = 0.5$. This increases the magnitude of the resultant electric field vector by $\approx 12\%$, the ion energy by $\approx 5\%$, and the N_2^+ ion collision frequency by $\approx 3\%$, and so decreases the drift velocity parallel to the laser beam by about 3%.
[48] W. P. Allis and D. J. Rose, Phys. Rev. **93**, 84 (1954); A. V. Phelps, J. Res. Natl. Inst. Stand. Tech. **95**, 407 (1991).
[49] G. Cernogora, L. Hochard, M. Touzeau, and C. M. Ferreira, J. Phys. B **14**, 2977 (1981).
[50] L. S. Polak, P. A. Sergeev, and D. I. Slovetskii, Teplofiz. Vys. Temp. **15**, 15 (1977) [High Temp. (USSR) **13**, 13 (1977)].
[51] A. Güntherschulze, Z. Phys. **42**, 718 (1927); **42**, 763 (1927). Güntherschulze assumed that all of the electron energy gained from the electric field, except that going to ionization, appears as translational-rotational energy. Boltzmann calculations [45] and our temperature rise measurements show that for near room temperature N_2 only 15–20% of the input energy appears as translational-rotational energy and that the remainder is transported to the wall as excited molecules, electron-ion pairs, or radiation. However, support for the assumption of efficient local energy relaxation for "hot" N_2 is provided by the temperature rise data of Polak, Sergeev, and Slovetskii [50]. Note that Güntherschulze assumed a radially uniform power input. Our comparison assumes a Bessel function power input and temperature profile corresponding to the expected electron density and assumes that we measure the peak temperature change.
[52] Recent papers include M. Waldman, E. A. Mason, and L. A. Vieland, Chem. Phys. **66**, 339 (1982); J. E. Lawler, Phys. Rev. A **32**, 2977 (1985).
[53] R. G. Breene, Appl. Opt. **6**, 141 (1967). We have scaled these results from 8000 K to 370 K using the temperature dependence expected for the Van der Waals interaction potential, i.e., $T^{-0.3}$.
[54] A. V. Phelps, J. Phys. Chem. Ref. Data **20**, 557 (1991).
[55] G. H. Wannier, *Statistical Physics* (Wiley, New York,

1966), p. 464.
[56] S. L. Lin and J. N. Bardsley, J. Chem. Phys. **66**, 435 (1977).
[57] J. T. Moseley, R. M. Snuggs, D. W. Martin, and E. W. McDaniel, Phys. Rev. **178**, 240 (1969). However, the values of D_T/μ for $E/n > 150$ Td are surprisingly low compared to, for example, those found for other symmetric charge transfer systems. See T. Stefánsson, T. Berge, R. Lausund, and H. R. Skullerud, J. Phys. D **21**, 1359 (1988) for He^+ in He; T. Stefánsson, J. Phys. B **22**, 3541 (1989) for Ne^+ in Ne; and H. R. Skullerud and P. -H. Larsen, J. Phys. B **23**, 1017 (1990) for theory.
[58] L. M. Chanin and M. A. Biondi, Phys. Rev. **106**, 473 (1957); E. W. McDaniel and E. A. Mason, *The Mobility and Diffusion of Ions in Gases* (Wiley, New York, 1973), Sec. 5-7.
[59] A. V. Phelps, J. Appl. Phys. (to be published).
[60] J. Borysow and A. V. Phelps, Bull. Am. Phys. Soc. **35**, 1837 (1990); J. Borysow and A. V. Phelps, *Abstracts of Contributed Papers, Seventeenth International Conference on the Physics of Electronic and Atomic Collisions*, edited by W. R. MacGillivray, I. E. McCarthy, and M. C. Standage, (AIP, New York, 1992).
[61] C. S. Gudeman and R. J. Saykally, Annu. Rev. Phys. Chem. **35**, 387 (1984); C. S. Gudeman, C. C. Martner, and R. J. Saykally, Chem. Phys. Lett. **122**, 108 (1985).
[62] C. P. Lauenstein, M. J. Bastien, V. M. Bierbaum, S. M. Penn, and S. R. Leone, J. Chem. Phys. **94**, 7810 (1991).
[63] Using the average N_2^+ - N_2 collision frequency calculated from mobility data [46], we obtain ion momentum relaxation times of $\approx 7 \times 10^{15}/n$ s, where n is the nitrogen density in m^{-3}.
[64] A uniform-weighting seven-point average is applied seven times to the original 50 ns/channel data to obtain the equivalent of smoothing with a Gaussian with a full width at half maximum of 16 points or 800 ns.
[65] A. G. Engelhardt, A. V. Phelps, and C. G. Risk, Phys. Rev. **135**, A1566 (1964).
[66] M. A. Biondi, in *Principles of Laser Plasmas*, edited by G. Bekefi (Wiley, New York, 1976), Chap. 4.
[67] A. J. Cunningham and R. M. Hobson, J. Phys. B **5**, 2328 (1972); P. M. Mul and J. Wm. McGowan, *ibid.* **12**, 1591 (1979).
[68] R. N. Varney, Phys. Rev. **174**, 165 (1968); D. Smith, N. G. Adams, and E. Alge, Chem. Phys. Lett. **105**, (1984).
[69] D. R. Bates, V. Malaviya, and N. A. Young, Proc. R. Soc. London Ser. A **320**, 437 (1971).
[70] D. R. Bates, in *Case Studies in Atomic Physics*, edited by M. R. C. McDowell and E. W. McDaniel (North-Holland, Amsterdam, 1974); D. R. Bates, J. Phys. B **13**, 2587 (1980).
[71] Numerical solutions to the rate equations for N_2^+ and N_4^+ justify the neglect of the N_4^+ ions in calculating the N_2^+ ion density decay. This occurs because the N_4^+ density is small when the recombination term involving the total ion or electron density is important.
[72] L. Frommhold and M. A. Biondi, Ann. Phys. (N.Y.) **48**, 407 (1968).
[73] A. Ershov and J. Borysow (unpublished).
[74] The photodissociation N_4^+ cross section peaks reach about 10^{-21} m^2 at near 320 nm, so that with our calculated maximum N_4^+ density of $\approx 10^{16}$ ions/m^3 and a 1 m absorption path (5 passes) one expects a fractional absorption of 10^{-5}. See G. P. Smith and L. C. Lee, J. Chem. Phys. **69**, 5393 (1978); S. C. Ostrander and J. C. Weisshaar, Chem. Phys. Lett. **129**, 220 (1986). Although a high energy pulsed laser will photodissociate N_4^+ and could produce an observable density ($\approx 10^{16}$ ion/m^3) of N_2^+, photoionization of excited N_2 probably would be a serious background problem. Another possibility is the weak photon induced fluorescence at $\lambda > 345$ nm with an $\approx 10^{-22}$ m^2 cross section for incident photons at $\lambda = 277$ nm.
[75] N. L. Alexsandrov, A. M. Konchakov, and É. E. Son, Fiz. Plasmy **4**, 1182 (1978) [Sov. J. Plasma Phys. **4**, 663 (1978)].
[76] H. Brunet, P. Vincent, and J. Rocca Serra, J. Appl. Phys. **54**, 4951 (1983); H. Brunet and J. Rocca Serra, *ibid.* **57**, 1574 (1985).
[77] P. J. Chantry, J. Appl. Phys. **62**, 1141 (1987).
[78] S. C. Saxena and P. K. Tondon, J. Chem. Eng. Data **16**, 212 (1971).
[79] See, for example, P. H. Vidaud, R. P. Wayne, M. Yaron, and A. von Engel, J. Chem. Soc. Faraday Trans. II **72**, 1185 (1976).
[80] R. Taylor and Bitterman, Rev. Mod. Phys. **41**, 26 (1969).
[81] F. Gilmore (private communication).
[82] From the diffusion coefficient for N in N_2 from H. I. Schiff as quoted by K. M. Evenson and D. S. Burch, J. Chem. Phys. **45**, 2450 (1966).
[83] Wall recombination coefficients of less than 10^{-5} have been reported for Pyrex, see, for example, Ref. [82] and T. Yamashita, J. Chem. Phys. **70**, 4248 (1979).
[84] F. Kaufman, Adv. Chem. **80**, 29 (1969).

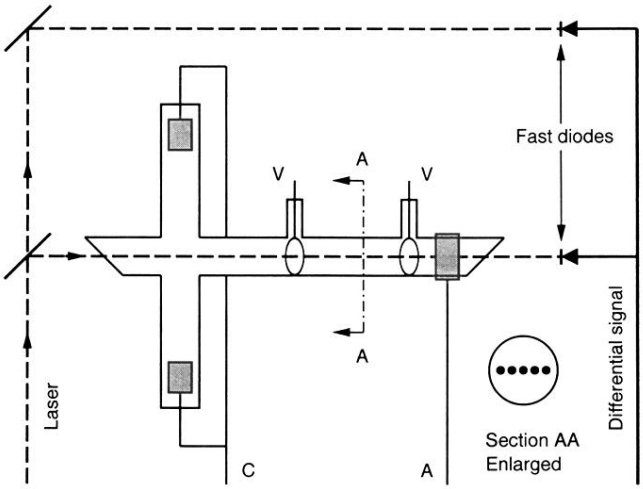

FIG. 1. Schematic of the experimental discharge tube used for Doppler shift and rotational population measurements in N_2. The solid circles in the section AA and the dashed line show the approximate location of the laser beams passing through the discharge. The arrows indicate the direction of the laser for the one-direction measurements. The voltage probes are labeled by V, the cathode connection by C, and the anode connection by A. The remainder of the circuitry and the optical system are described in Ref. [27].